AFRICA JOURNAL OF PHYSICAL SCIENCES

Africa Journal of Physical Sciences Vol. 3, pp. 39-54, February 2019

http://journals.uonbi.ac.ke/index.php/ajps/index

ISSN 2313-3317

Device Simulation of Sb_2S_3 Solar Cells by SCAPS-1D Software

ODARI, Victor [1,2a]*, MUSEMBI, Robinson [1, b] and MWABORA Julius [1, c]

[1]Department of Physics, School of Physical Sciences, University of Nairobi, P.O. Box 30197-00100 Nairobi, Kenya.

[2]Department of Physics, School of Natural and Applied Sciences, Masinde Muliro University of Science and Technology, P.O. Box 190-50100 Kakamega, Kenya.

[a]vodari@mmust.ac.ke*, [b]musembirj@uonbi.ac.ke, [c]mwabora@uonbi.ac.ke

ARTICLE INFO

Article History:

Submitted: 22 Jan 2015

Accepted: 9 Sep 2018

Available online: 28 February 2019

Keywords:

Antimony Sulphide (Sb_2S_3)

Processing parameters

Simulation

SCAPS software

ABSTRACT

Antimony sulphide (Sb_2S_3) has drawn research interest due to its promising properties for photovoltaic applications. The progress in developing highly efficient Sb_2S_3 solar cells has stimulated this study to a great extent. In this paper, we present the results of a simulation of solar cell processing parameters on the performance of the solar cell through theoretical analysis and device simulation using SCAPS software. The results of this simulation show that the solar cell performance can be enhanced to a great extent by adjusting the thickness, doping concentration and defect density of both the TiO_2 buffer layer and Sb_2S_3 absorber layer and also the electron affinity of the TiO_2 buffer layer. Optimized parameters were found to be: doping concentration of ($1.0 \times 10^{17} cm^{-3}$ for TiO_2 and $3.0 \times 10^{16} cm^{-3}$ for Sb_2S_3), defect density of the Sb_2S_3 absorber at ($1.0 \times 10^{15} cm^{-3}$) and the electron affinity of the buffer layer at (4.26 eV). The results obtained were as follows: V_{oc} of 750 mV, J_{sc} of 15.23 mA/cm^2, FF of 73.55% and efficiency of 8.41%. These results show that Sb_2S_3 is a potential earth-abundant compound that can yield highly efficient solar cells.

ISSN 2313-3317, Vol 3

1. Introduction

Antimony sulphide (Sb_2S_3) is a chalcogenide semiconductor with promising properties for photovoltaic applications such as its suitable band gap, relatively non-toxic and earth-abundant constituent, simple composition (binary compound), and long term stability [1].

It is a V–VI semiconductor material and exists in nature in the form of the mineral stibnite with orthorhombic crystal structure (lattice parameters *a* = 1.1239; *b* = 1.1313; and *c* = 0.38411 nm) [2]. It has been widely used in electronic applications such as thermoelectric devices, photo-electrochemical cells, microwave devices, switching devices and photodetectors [3]. Various techniques such as thermal evaporation [3–6], chemical bath deposition [7–10], spin coating [11], spray pyrolysis, sputtering [12] and electrodeposition [13] have been used to deposit Sb_2S_3 thin films. Depending on the method of synthesis, both p-type and n-type conductivity have been reported for Sb_2S_3 thin films [13].

Many research groups have demonstrated the use of Sb_2S_3 as an absorber material either as a planar or a sensitized solar cell [3, 12]. Efficiencies up to 1.27% have been reported using thermally evaporated Sb_2S_3 absorber layer [2]. [11] report an approach based thermal decomposition of $Sb(III)(thioacetamide)_2Cl_3$ that yielded solar cells with a short-circuit current density of 8.12 $mAcm^{-2}$ and an efficiency of 2.39% [11]. [14] reported a conversion efficiency of 5.1% for aqueous Sb_2S_3 deposited at room temperature by CBD. [14] and [15] reported Sb_2S_3 by CBD on nanoporous TiO_2 and organic hole transporting material yielded an efficiency of 5.2%. [8] reported a photocurrent density of 16.3mA/cm^2 and power conversion efficiency of 5.7% for a glass/FTO/TiO_2/Sb_2S_3/CuSCN/Au structure using Sb_2S_3 doped with 5 at% Ti as a thin absorber film [8]. The highest efficiency of 7.5% has been achieved with a TiO_2/Sb_2S_3 based heterojunction system of the type: mesoporous-TiO_2/Sb_2S_3/PCPDTBT (poly(2,6-(4,4-bis-(2-ethylhexyl)-4Hcyclopenta[2,1b;3,4-b′] dithiophene)-alt-4,7(2,1,3-benzothiadiazole))/Au [16].

In spite of the improvement in efficiencies of the Sb_2S_3 based solar cells, to date, there has been no report on their device simulation which can apprise experimentalist on the possible maximum limit for this material. Simulation methods allow instinctive analysis of each parameter in solar cells and thus identify the optimal conditions of operation [17 - 18]. This study therefore focuses on factors that affect the performance of planar Sb_2S_3 based solar cells which include film thickness, defect density and doping density variation of Sb_2S_3 absorber layer and the thickness, doping density and electron affinity of the TiO_2 buffer layer using the one-dimensional device simulation with the solar cell capacitance simulator (SCAPS) version 3.3.03 [19] under AM1.5G illumination. SCAPS is based on three semiconductor equations and can model various homo-junctions, hetero-junctions, multi-junctions and Schottky barrier devices [17].

2. Numerical Modeling and Material Parameters

The one dimensional SCAPS software [19] allows simulation of planar devices. The Sb_2S_3 based planar solar cell with layer configuration of glass substrate/TCO/Buffer layer of TiO_2 /absorption layer Sb_2S_3/hole transport material (HTM) P3HT/ Ag back contact is shown in figure 1. The material parameters of the different layers have been selected from those reported in theoretical and experimental data of other works [20]. Table 1 summarizes the parameters of each layer in the architecture and also indicates the parameters that were optimized for better results. Sb_2S_3 is said to have a number of defects which include sulphur vacancies and antimony interstitials [21]. Therefore, we set the absorption characteristic energy at 0.1 eV and introduce two levels antisite defects Sb_{S2} in the band gap, one donor at ∈SbS 2 (+/0) = 0.28 eV and one acceptor at ∈SbS 2 (0/−) = 0.53 eV, which are both above VBM and should dislocate E_F near the VBM inducing p-type conductivity [21]. The initial defect density N_t of Sb_2S_3 absorber material is set to 5.000E+14 [16]. The defects in Sb_2S_3 as outlined by [21] show a p-type conducting behavior.

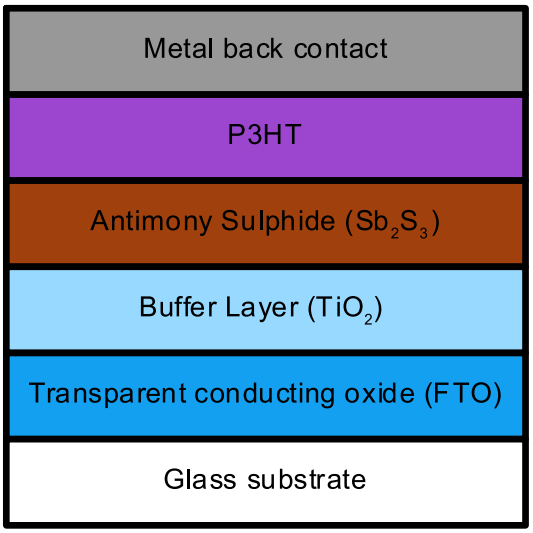

Figure 1: Cell architecture of planar Sb_2S_3 based solar cell

Table 1. Layer parameters for the different layers of a Sb_2S_3-based solar cell at 300 K.

Parameter	Units	FTO	cp-TiO_2	Sb_2S_3	P3HT
E_g (Band gap)	eV	3.5	3.2	1.7	2
χ_e (Electron affinity)	eV	4.4	4.26 (Varied)	3.8	3.2
***w* (Thickness)**	nm	500	50 (Varied)	80 (Varied)	100
ε_r (Permittivity)		9	11.9	7	3
μ_n (electron mobility)	cm^2 /Vs	20	20	7.0×10^{-2}	6.0×10^{-2}
μ_p (hole mobility)	cm^2 /Vs	10	10	2.0×10^{-2}	1.0×10^{-2}
N_C (Effective density of states in the conduction band)	cm^{-3}	2.2×10^{18}	2.2×10^{18}	1.0×10^{19}	1.0×10^{19}
N_V (Effective density of states in the valence band)	cm^{-3}	1.8×10^{19}	1.8×10^{19}	1.0×10^{19}	1.0×10^{19}
N_A (Carrier density of the acceptor)	cm^{-3}	0	0	3.0×10^{16}(Varied)	3.0×10^{16}
N_D (Carrier density of the donor)	cm^{-3}	2.0×10^{19}	1.0×10^{16}	0	0

We, therefore, assume that the absorber is p-type semiconductor with initial carrier density of 3.000E+16 cm^{-3}. We have also introduced bulk defects in each layer as shown in Table 2. The interface defect at the TiO_2/Sb_2S_3 interface is set to be a neutral defect with a total density of 2.50E+17 [22] and single energetic distribution below the lowest E_c as shown in Table 3.

The absorption coefficient (α) curve is calculated from $\alpha = A_\alpha \left(h\nu E_g\right)^{1/2}$ with the pre-factor A_α set to 10^5.

Table 2. Parameters for the Gaussian distributed defect states in the different layers of Sb_2S_3 solar cell.

	Units	FTO	cp-TiO_2	Sb_2S_3
Type		Neutral	Neutral	Donor
Density of defects	cm^{-3}	$1\times10^{+15}$	$1\times10^{+15}$	Varied from 10^{10} to10^{19}
Electron capture cross-section (σ_n)	cm^2	1×10^{-15}	1×10^{-19}	1.34×10^{-17}
Hole capture cross-section (σ_p)	cm^2	1×10^{-15}	1×10^{-19}	1.34×10^{-17}
Energy	eV	Above E_V	Above E_V	Above E_V

Table 3. Interface properties in Sb_2S_3 solar cells.

	Interface	TiO_2/Sb_2S_3
Parameter	Type	Neutral
Density of defects	cm^{-2}	2.50×10^{17}
electron capture cross-section (σ_n)	cm^{-2}	2.21×10^{-9}
hole capture cross section (σ_p)	cm^{-2}	2.21×10^{-9}
Energy	eV	Below the lowest E_C

Table 4 shows the solar cell parameters of the best cell of Sb_2S_3 [16] that has so far been reported and the parameters of our simulated cell that mimic it using the initial parameters in table 1. The short-circuit current density (J_{sc}) of 14.77 mA/cm^2, open-circuit voltage (V_{oc}) of 711.1 mV, fill factor (FF) of 71.82% and power conversion efficiency (PCE) of 7.54% are obtained. These simulated device parameters differ by a negligible error with the experimental values indicating that the device simulation is valid and the input parameters that have been set are close to those for a real device.

Table 4. Simulation and experiment parameters of a Sb_2S_3 cell.

	V_{OC}(mV)	J_{SC}(mA/cm^2)	FF (%)	η (%)
Experiment [16]	711	16.1	65	7.5
SCAPS Simulation	711.1	14.77	71.82	7.54

3. Results and Discussions

3.1 Effect of buffer layer thickness on the *J-V* characteristics

The simulation started by setting the thickness of Sb_2S_3 layer to 200 nm and varying the thickness of the TiO_2 buffer layer from 40 nm to 200 nm. It was observed that an increase in the thickness of the buffer layer leads to deteriorating solar cell properties as seen in figure 1. The significant change in the V_{oc}, *FF* and efficiency of the cells is as a result of increase in the length of the electron pathways in TiO_2 which in extreme cases causes decrease in J_{sc}. This change in V_{oc} can also be due to unnecessary increase in the total TiO_2 surface area, causing electron back transfer reaction as shown in Figure 2. J_{sc} can also decrease because fewer photons penetrating to the Sb_2S_3 absorber layer when the thickness of the buffer layer is increased as shown in the graph of quantum efficiency in Figure 3. The generated charges need to have a longer lifetime to be extracted through the TiO_2 buffer layer but that is not possible. Consequently, there is increase in charge recombination occurring slightly at the absorber layer and more in the buffer layers as shown in Figure 4 as a result of increase in diffusion length with increase in TiO_2 thickness. Thin buffer layers of less than 40 nm may not be achieved experimentally due to instruments limitations or the required fabrication techniques [18, 23]. Therefore, the range of 40 nm to 50 nm is the preferred optimized thickness of the TiO_2 buffer layer for Sb_2S_3 based solar cell.

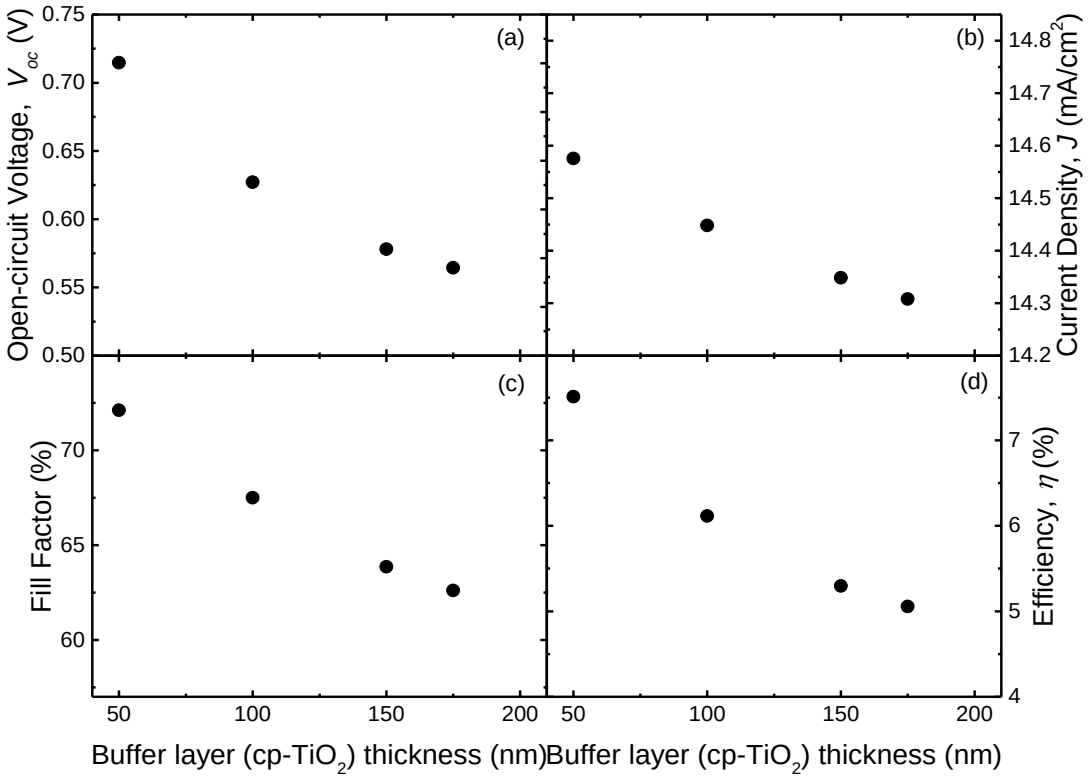

Figure 2: Variation in solar cell parameters with thickness of the buffer layer. There is increase in recombination at the TiO_2 layer due to the short carrier lifetime with increase in thickness.

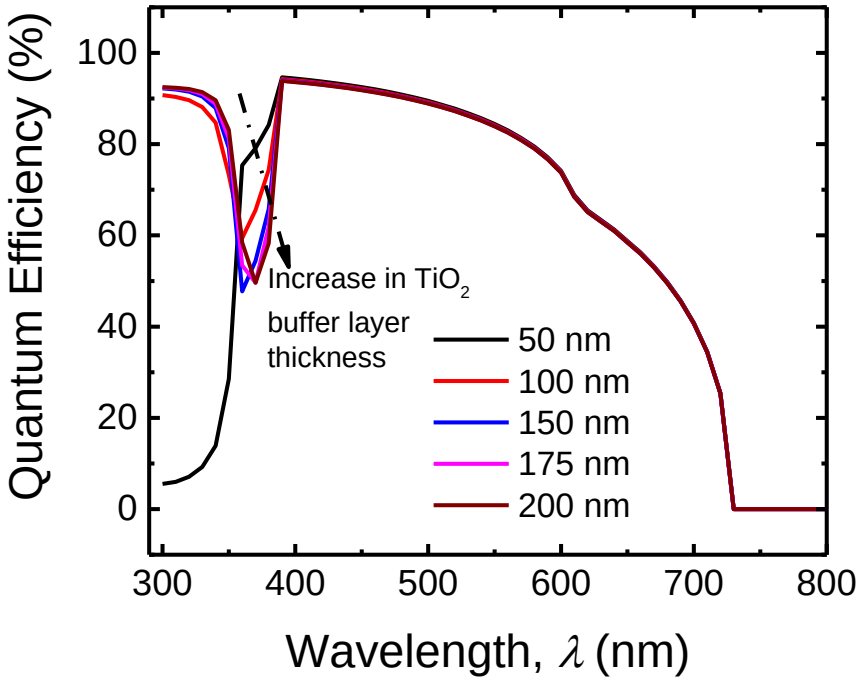

Figure 3: Quantum efficiency for Sb_2S_3 solar cells with varying thickness of the TiO_2 buffer layer

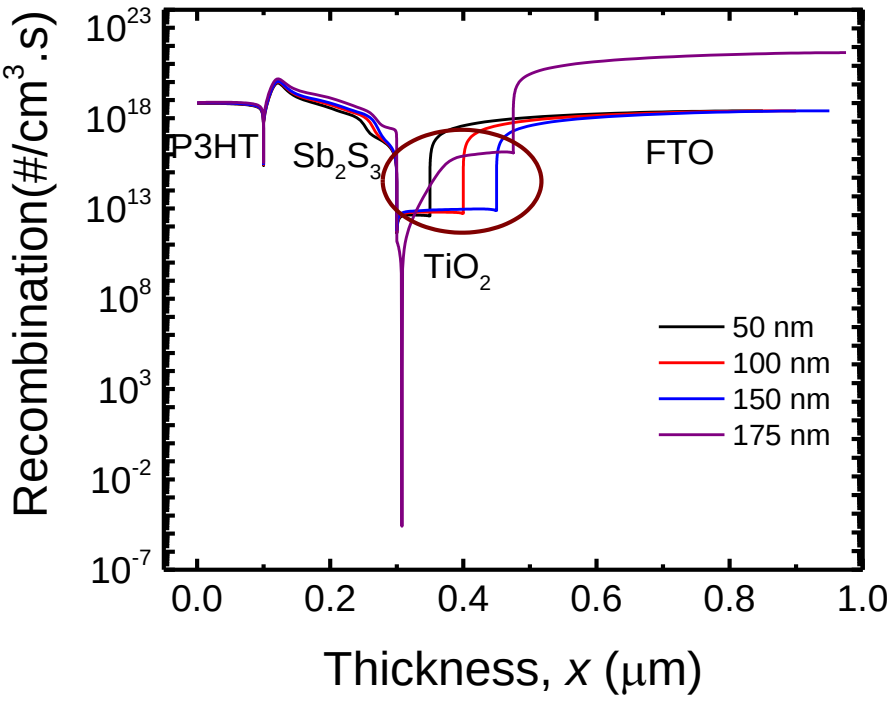

Figure 4: Recombination of charges with increase in buffer layer thickness

3.2 Effect of varying buffer layer (TiO_2) doping density

Figure 5 shows increase in the doping density of the buffer layer results in improvement in the open-circuit voltage, fill factor and eventually the efficiency of the cells. Doping of the buffer layer mainly affects the reverse saturation current and the overall solar cell conversion efficiency.

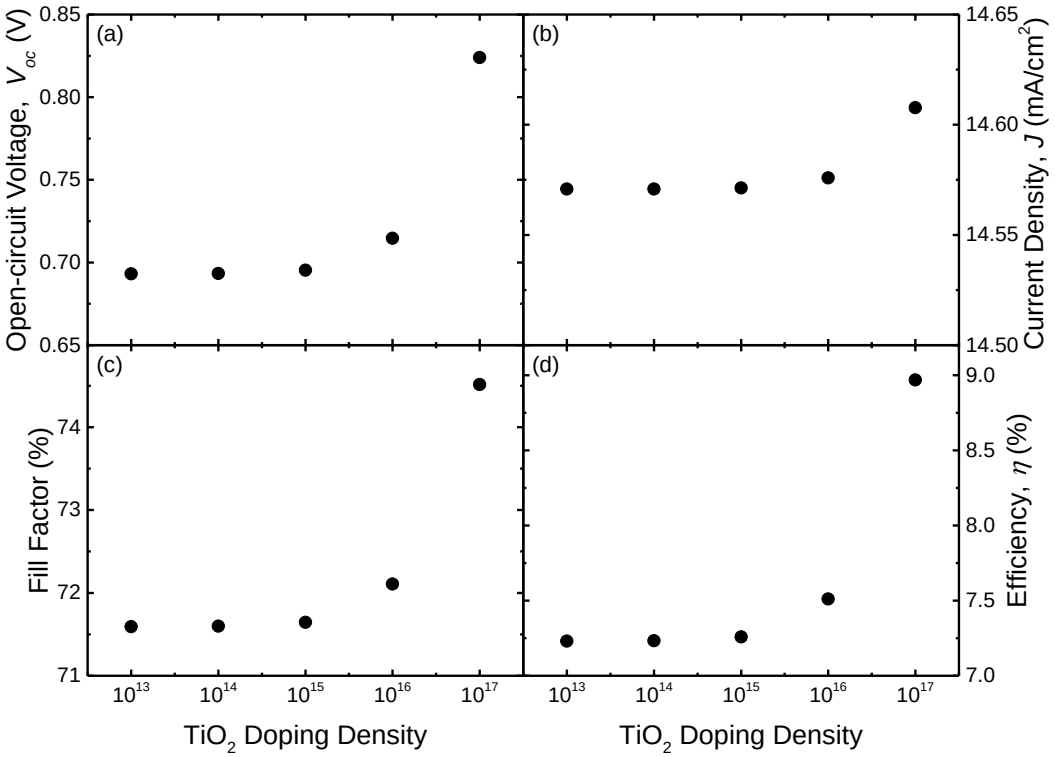

Figure 5: Variation in solar cell parameters with doping density of the buffer layer. Increase in the doping density leads to improved solar cell performance.

As the doping density increases from relatively small values of 10^{13} per cm^3, the reverse saturation current decreases leading to an increase in the open circuit voltage and consequently the conversion efficiency. This increase is sustained until the high doping effects appear causing a reduction of the band gap and the minority carrier life time which are expected to cause the reverse saturation current to decrease further after reaching a peak with the doping concentration in the TiO_2. The slight decrease in band gap and minority carrier lifetime, therefore, leads to no significant change in the current density as shown by the graph of quantum efficiency in Figure 6. The doping concentrations as a process parameter therefore positively affects the open circuit voltage in the sense that the open circuit voltage increases by increasing the doping to an optimum value. These results show that doping densities of 10^{17} per cm^{-3} can yield solar cell efficiency of ~ 9% for the solar cell structure in Figure 1. Doping densities above this value may hardly change its carrier concentration given that TiO_2 is intrinsically an n-type semiconductor with high electron concentration.

It is expected that for an increase in defect density, both minority carrier lifetime and mobility should decrease causing a decrease in the open-circuit voltage but this has no effect on the TiO_2 buffer layer as shown in Figure 7.

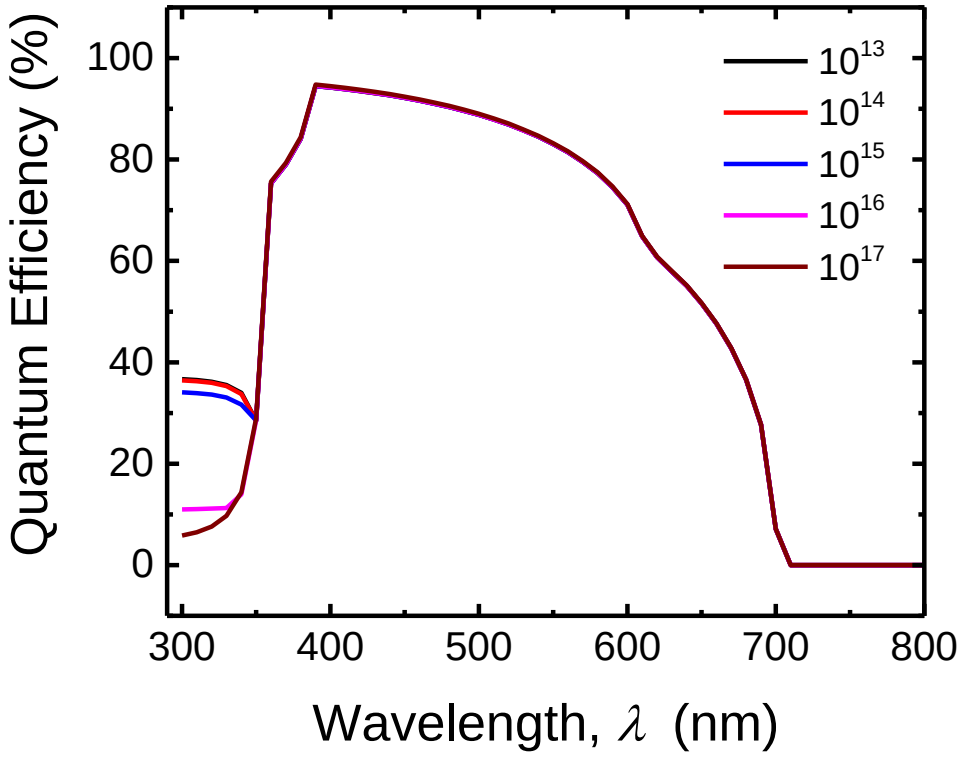

Figure 6: Quantum efficiency of solar cells with varying TiO_2 doping density.

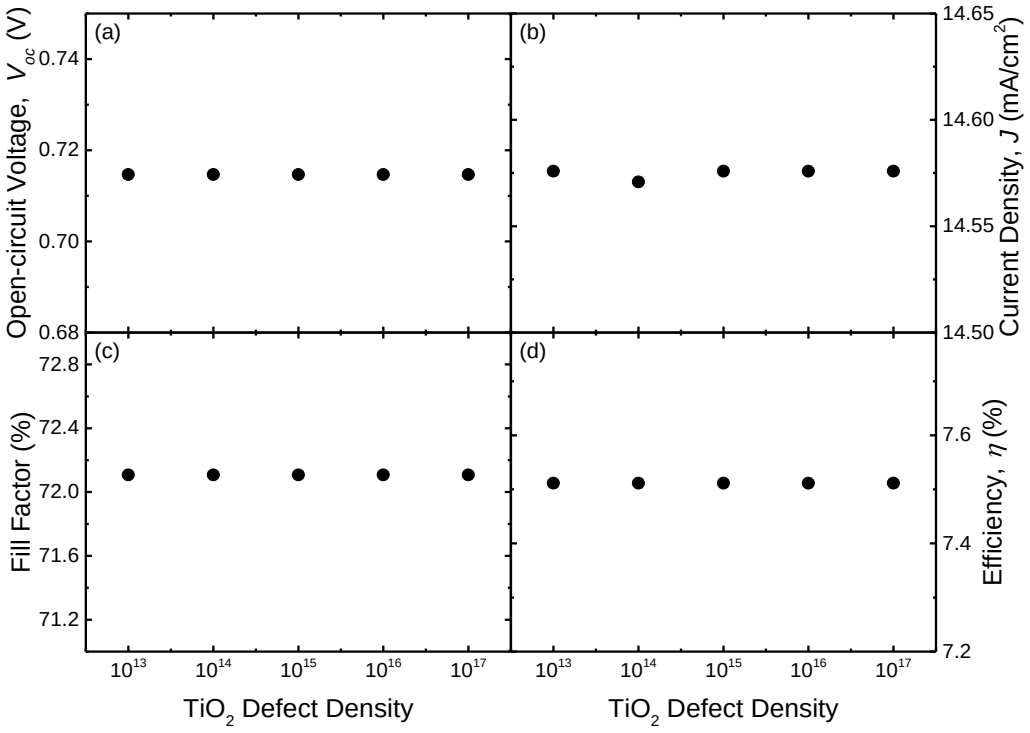

Figure 7: Graph on the effect of varying defect density of the TiO_2 buffer layer on the solar cell parameters.

3.3 Effect of varying buffer layer (TiO_2) electron affinity

A critical factor of carrier recombination at the interface of semiconductors which determine the open-circuit voltage is the band offset between buffer/absorption layer/HTM [17]. We adjusted it by varying the values of electron affinity (χ) of the buffer from 3.5 eV to 4.7 eV. The variations of V_{oc}, J_{sc}, *FF*, and *PCE* with electron affinity value are shown in Figure 8. Satisfactory results of the solar cell parameters can be obtained at the χ values of 3.5 eV– 4.2 eV for the buffer layer. A notch is formed on the hole Fermi level at the interface of the buffer layer and absorber as shown in the inset of Figure 9. The position of this notch with respect to the vacuum level, increases with increase in the electron affinity for energy values greater than 4.2 eV. The notch for the χ values of 4.2 eV and 4.4 eV are -0.39eV and -0.28 eV respectively, indicating a high probability of carrier recombination at the interface hence causing a decrease in the V_{oc}.

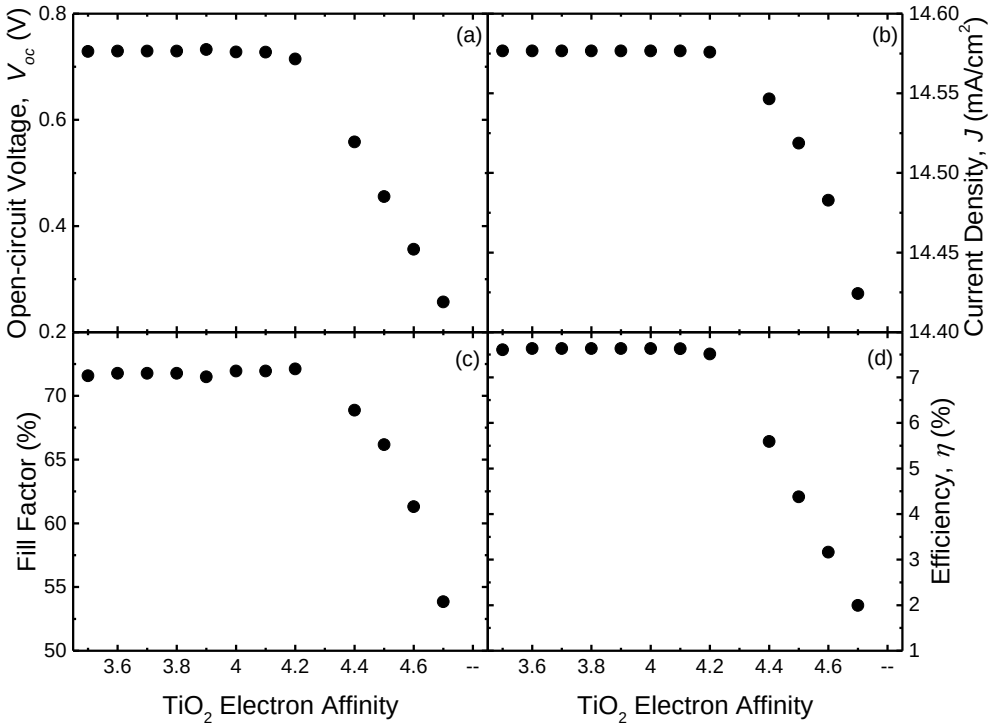

Figure 8: Variation in solar cell parameters with TiO_2 electron affinity. There is no significant change in the cell parameters for layers with electron affinity of 4.2 eV and below.

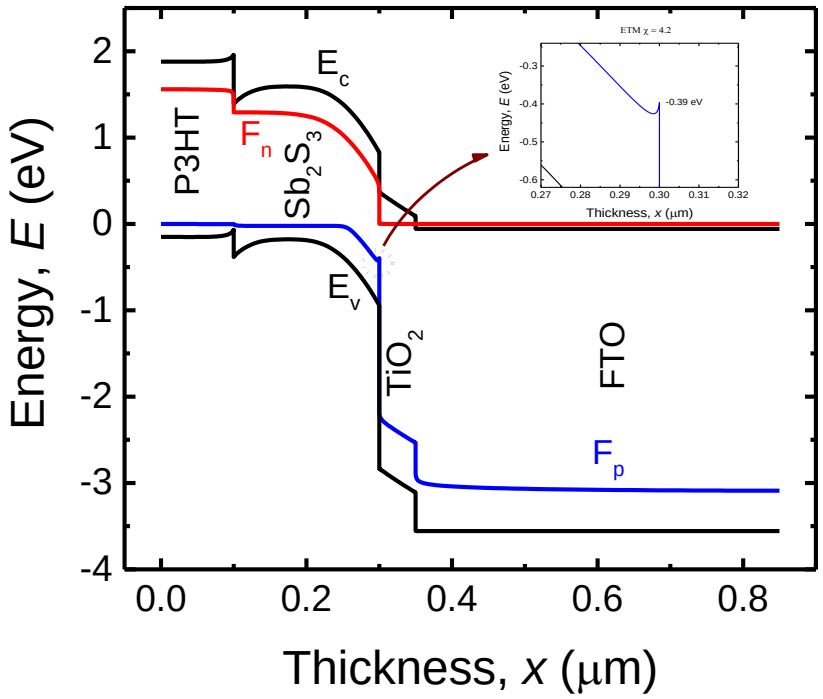

Figure 9: Band diagram of Sb_2S_3 solar cell with TiO_2 buffer layer

3.4 Effect of Sb_2S_3 thickness on the photovoltaic parameters

The thickness of the absorber layer plays an important role in charge extraction in thin films and the layer must be made sufficiently large to absorb all the penetrating incident radiation. This can be varied in the fabrication process. To obtain qualitative information, we have investigated the effects of Sb_2S_3 layer thickness on the performance of the solar cells. Figure 10 shows variations in the solar cell parameters when varying the thickness of Sb_2S_3 layer while keeping other layer properties constant. We observe that the V_{oc} and *FF* are nearly constant for thickness beyond 140 nm while the J_{sc} and the cell efficiency increase exponentially. Increase in thickness of the absorber layer, as expected, causes an increase in the short-circuit current resulting from more photons that are absorbed by Sb_2S_3 layer. This also causes an increase in recombination of charges both at the interface of Sb_2S_3/P3HT and in the bulk of Sb_2S_3 as seen in Figure 11. These recombination lead to a drop in the V_{oc} to a nearly constant value of 0.7 V for thickness beyond 140 nm. This value of thickness was also reported by [10] for chemically deposited n-type Sb_2S_3 as the hole ambipolar diffusion length together with the electron diffusion length of ~1 μm [10]. The obtained almost constant V_{oc} is due to the recombination kinetics in Sb_2S_3 is not expected to change when the diffusion length of charge carriers gets significantly lower than the thickness of the layer [10] implying that recombination is not affected by the surface states in Sb_2S_3. Recombination of the charge carriers is therefore due to defects at grain boundaries and in the bulk of the material.

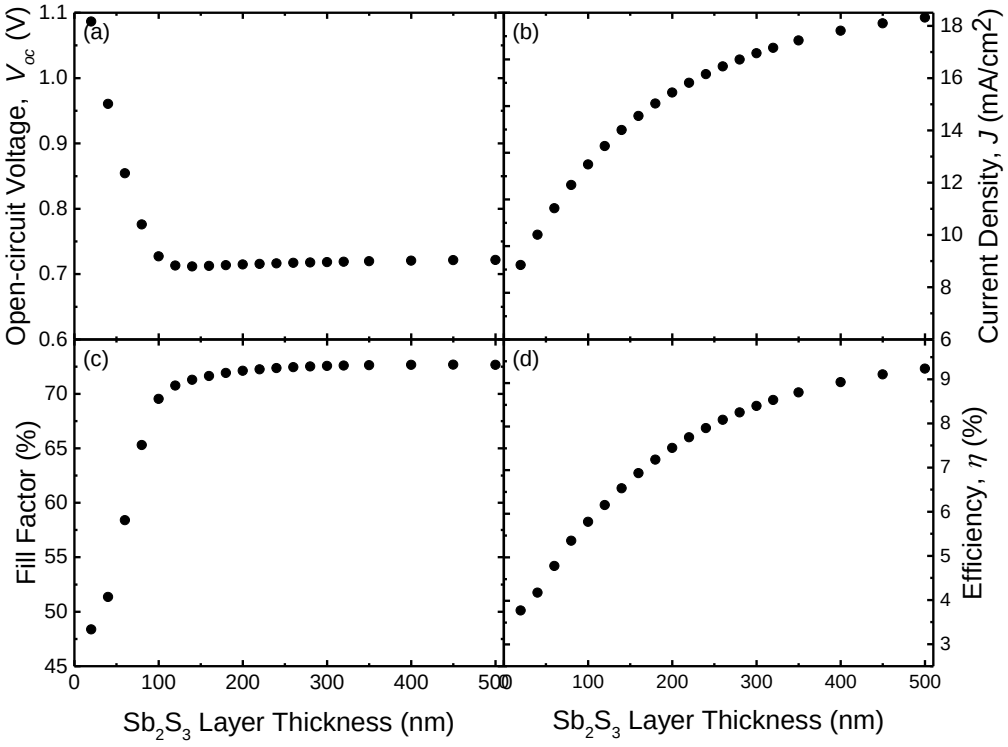

Figure 10: Variation in solar cell parameters with thickness of Sb_2S_3. Thicker films have a fairly constant output.

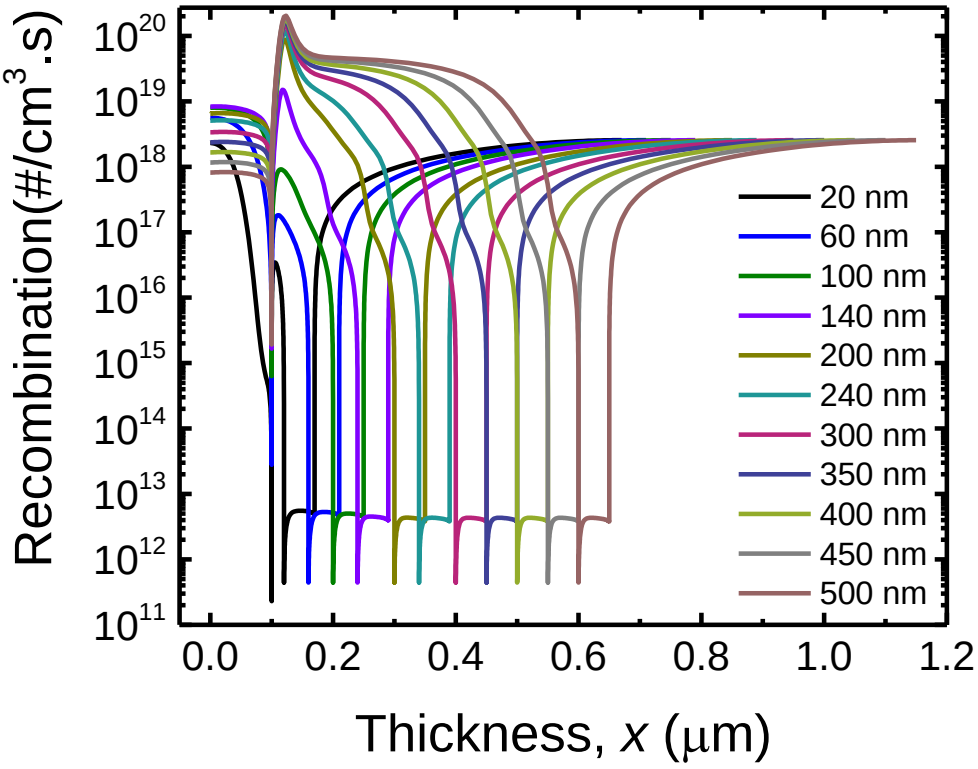

Figure 11: Recombination rate verses Sb_2S_3 thickness.

3.5 Effect of Sb_2S_3 defects density on the photovoltaic parameters

Milton *et al*. [21] have theoretically studied the defect properties of Sb_2S_3 using the density functional theory calculations in VASP software and reported on native point defects which may determine the type of Sb_2S_3 semiconductor. Their study show that a p-type Sb_2S_3 semiconductor can be obtained from low formation energy of antisite defects of Sb_S^2 (Sb in place of S2 atom), introducing two levels in the band gap. These levels are a single donor (+/0) at 0.28 eV and a single acceptor (0/-) at 0.53 eV which are above the valence band maximum and will dislocate E_F near the VBM. Figure 12 presents the defect density effects on the solar cell performance parameters using the results obtained by Milton *et al*. The performance of the solar cell is at its best when the defects density is below 10^{15} cm^{-3}. When the defects density exceeds this value, the electrical performance of all the parameters are strongly affected. The presence of oxygen ions in chemical bath deposited Sb_2S_3 may also introduce carrier traps which result in weak efficiency solar cells. Roy *et al*. [24]reported two activation energy for p-type Sb_2S_3 of 0.40 and 0.22 eV which correlate to the donor level at 0.28 eV and acceptor level at 0.53 eV [16], [21] and are lower than its band gap (1.7 eV). Thus, close to deep defect levels, increase of defect density contributes to recombination loss mechanism. Therefore, fabrication of Sb_2S_3 absorber materials with a high quality (defect density ~10^{15} cm^{-3}) is important for the Sb_2S_3 based solar cell devices.

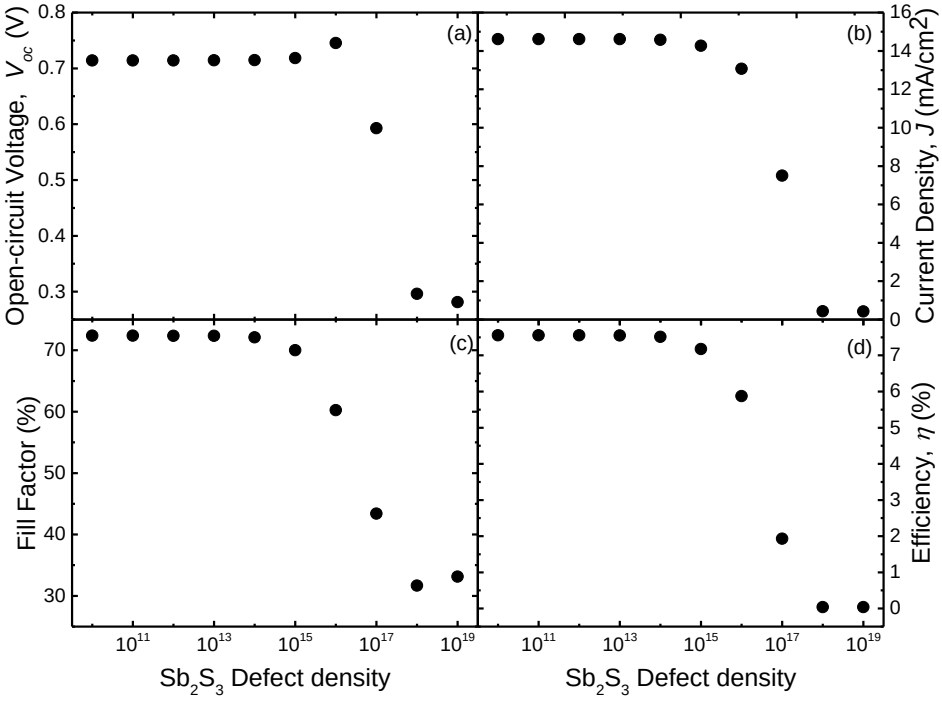

Figure 12: Variation in solar cell parameters with defect density of Sb_2S_3.

3.6 Effect of doping density in Sb_2S_3 solar cells

Figure 13 illustrates the influence of the holes' density (p) on V_{oc}, J_{sc}, FF, and efficiency of Sb_2S_3 solar cell. We obtained a nearly constant open-circuit voltage of 0.9 V, short-circuit current of 13.9 mA/cm^2, fill factor of 46% and efficiencies of 6% for doping densities of less than 10^{14} cm^{-3}. Doping densities higher than this value has improved solar cell parameters apart from the V_{oc}. Increase in doping densities reduces the trap density in Sb_2S_3 and therefore improves on charge collection from the absorber.

Doping densities above 10^{14} cm^{-3} will result in decrease in V_{oc} but with improvement in J_{sc}, FF and efficiency of the cells. This is a result of a shift in the Fermi levels towards the mid-gap hence lowering the V_{oc} and enabling easy excitation of charges. Doping densities above 10^{16} cm^{-3} may not improve the cell efficiency and therefore, to get efficiencies above 7.5 %, other parameters have to be optimized.

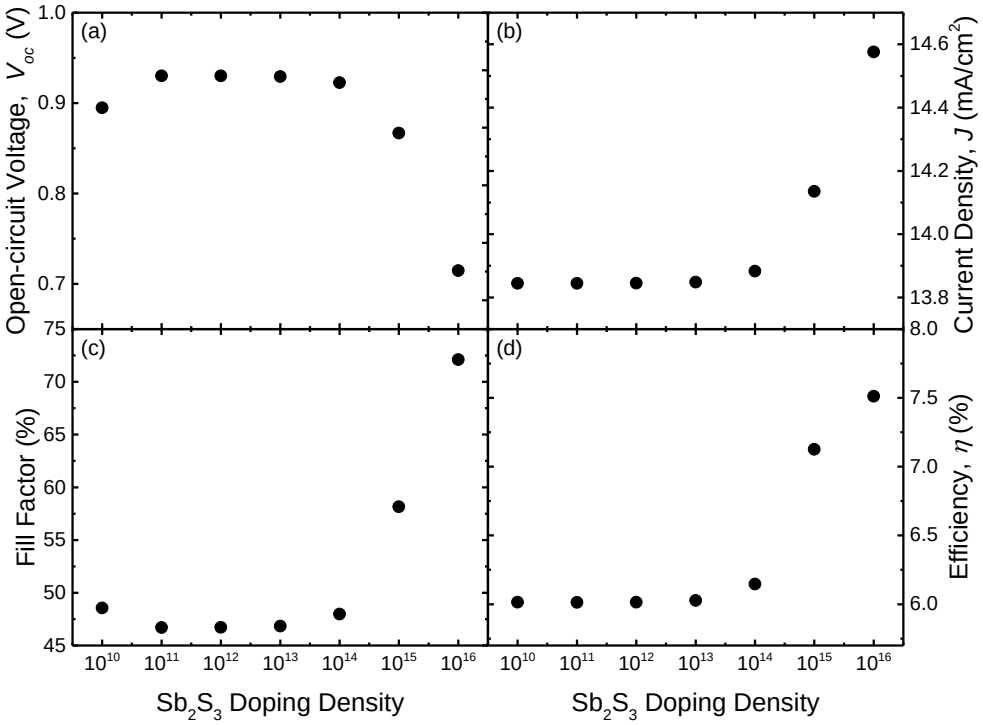

Figure 13 Variation in solar cell parameters with doping density of Sb_2S_3.

Finally, we considered all the optimum values obtained in sub-sections 3.1 – 3.6 (see Table 5) and obtained encouraging results of the V_{oc} of 750.8 mV, J_{sc} of 15.23 mA/cm^2, *FF* of 73.55% and PCE of 8.41% as shown in Table 6. These results show that Sb_2S_3 solar cells with high efficiency can be achieved by optimizing the thickness and doping densities of both the TiO_2 buffer layer and Sb_2S_3 absorber layer, the electron affinity of TiO_2 and more importantly the defects in Sb_2S_3 which is the main challenge for Sb_2S_3 absorber layer.

Table 5. Final optimized parameters of Sb_2S_3 solar cell with TiO_2 buffer layer

Parameter	Units	cp-TiO_2	Sb_2S_3
X_e (Electron affinity)	eV	4.26	_
w (Thickness)	nm	50	140
Density of defects	cm^{-3}	No change	1.0×10^{15}
N_A (Carrier density of the acceptor)	cm^{-3}	_	3.0×10^{16}
N_D (Carrier density of the donor)	cm^{-3}	1.0×10^{17}	_

Table 6. Results for optimized parameters of Sb_2S_3 solar cell with TiO_2 buffer layer

	V_{OC}(mV)	J_{SC}(mA/cm^2)	FF (%)	η (%)
Experiment [Choi *et al*, 2014]	711	16.1	65	7.5
SCAPS Simulation (Start)	714.7	14.58	72.11	7.51
SCAPS Simulation (Final)	750.8	15.23	73.55	8.41

4. Conclusions

Sb_2S_3 solar cell performance is simulated and analyzed by the functions of the buffer layer and the absorber layer. The optimum thickness of the Sb_2S_3 absorber layer and the TiO_2 buffer layer are found in the range of 130nm to 150nm and between 40nm and 50nm respectively. Increase in thickness of the buffer layer deteriorates the performance of the solar cell due to an increase in the length of electron pathways in TiO_2 and fewer photon penetration to the absorber layer. This leads to increase in recombination and electron back transfer reaction. Variation in doping density of buffer layer affects only the open circuit voltage while variations in defect density has no significant effect on the performance of the cell. Increasing the thickness of the Sb_2S_3 absorber layer leads to increase in the short circuit current but with decrease in the open circuit voltage to a nearly constant 0.7 V due to increase in recombination kinetics at the interface and in the bulk of Sb_2S_3.

Increase in doping densities reduces the trap density in Sb_2S_3 and therefore improves on charge collection from the absorber. These results can be used to obtain a highly improved thin film Sb_2S_3 solar cell but there is need to optimize the fabrication process so as to achieve the above results.

5. Acknowledgements

The authors would like to acknowledge financial support from International Science Programme (ISP) and DAAD for research facilitation and Ph.D. scholarship at University of Nairobi respectively. They also thank Professor Marc Burgelman and his colleagues in the Department of Electronics and Information Systems, University of Gent for the development of the SCAPS software package and allowing its use.

References

[1] Abulikemu, M., S. D. Gobbo, D. H. Anjum, M. A. Malik, and O. M. Bakr, (2016) Colloidal Sb2S3 nanocrystals: synthesis, characterization and fabrication of solid-state semiconductor sensitized solar cells: Journal of Materials Chemistry A, **4(18)**: 6809–6814, doi:10.1039/C5TA09546H.

[2] Escorcia-García, J., D. Becerra, M. T. S. Nair, and P. K. Nair, (2014) Heterojunction CdS/Sb2S3 solar cells using antimony sulfide thin films prepared by thermal evaporation: Thin Solid Films, **569**: 28–34, doi:10.1016/j.tsf.2014.08.024.

[3] Sotelo Marquina, R. G., T. G. Sanchez, N. R. Mathews, and X. Mathew, (2017) Vacuum coated Sb2S3 thin films: Thermal treatment and the evolution of its physical properties: Materials Research Bulletin, **90**: 285–294, doi:10.1016/j.materresbull.2017.03.013.

[4] Lakhdar, M. H., B. Ouni, and M. Amlouk, (2014) Thickness effect on the structural and optical constants of stibnite thin films prepared by sulfidation annealing of antimony films: Optik, **125** (10): 2295–2301, doi:10.1016/j.ijleo.2013.10.114.

[5] Yuan, S., H. Deng, D. Dong, X. Yang, K. Qiao, C. Hu, Huaibing Song, Haisheng Song, Z. He, and J. Tang, (2016) Efficient planar antimony sulfide thin film photovoltaics with large grain and preferential growth: Solar Energy Materials and Solar Cells, **157**:887–893, doi:10.1016/j.solmat.2016.07.050.

[6] Deng, H., S. Yuan, X. Yang, F. Cai, C. Hu, K. Qiao, J. Zhang, J. Tang, H. Song, and Z. He, (2017) Efficient and stable TiO2/Sb2S3 planar solar cells from absorber crystallization and Se-atmosphere annealing: Materials Today Energy, **3**:15–23, doi:10.1016/j.mtener.2017.02.001.

[7] Shaji, S., L. V. Garcia, S. L. Loredo, B. Krishnan, J. A. Aguilar Martinez, T. K. Das Roy, and D. A. Avellaneda, (2017) Antimony sulfide thin films prepared by laser assisted chemical bath deposition: Applied Surface Science, **393**:369–376, doi:10.1016/j.apsusc.2016.10.051.

[8] Ito, S., K. Tsujimoto, D.-C. Nguyen, K. Manabe, and H. Nishino, (2013) Doping effects in Sb2S3 absorber for full-inorganic printed solar cells with 5.7% conversion efficiency: International Journal of Hydrogen Energy, **38**(36):16749–16754, doi:10.1016/j.ijhydene.2013.02.069.

[9] Mushtaq, S., B. Ismail, M. Aurang Zeb, N. J. Suthan Kissinger, and A. Zeb, (2015) Low-temperature synthesis and characterization of Sn-doped Sb2S3 thin film for solar cell applications: Journal of Alloys and Compounds, **632**:723–728, doi:10.1016/j.jallcom.2015.01.307.

[10] Darga, A., D. Mencaraglia, C. Longeaud, T. J. Savenije, B. O'Regan, S. Bourdais, T. Muto, B. Delatouche, and G. Dennler, (2013) On Charge Carrier Recombination in Sb2S3 and Its Implication for the Performance of Solar Cells: The Journal of Physical Chemistry C, **117**(40):20525–20530, doi:10.1021/jp4072394.

[11] You, M. S., C.-S. Lim, D. H. Kwon, J. H. Heo, S. H. Im, and K. J. Chae, (2015) Oxide-free Sb2S3 sensitized solar cells fabricated by spin and heat-treatment of Sb(III)(thioacetamide)2Cl3: Organic Electronics, **21**:155–159, doi:10.1016/j.orgel.2015.02.015.

[12] Gao, C., M. Xu, B. K. Ng, L. Kang, L. Jiang, Y. Lai, and F. Liu, (2017) In situ growth of Sb2S3 thin films by reactive sputtering on n-Si(100) substrates for top sub-cell of silicon based tandem solar cells: Materials Letters, v. 195, p. 186–189, doi:10.1016/j.matlet.2017.02.046.

[13] Avilez Garcia, R. G., C. A. Meza Avendaño, M. Pal, F. Paraguay Delgado, and N. R. Mathews, (2016) Antimony sulfide (Sb_2S_3) thin films by pulse electrodeposition: Effect of thermal treatment on structural, optical and electrical properties: Materials Science in Semiconductor Processing, **44**:91–100, doi:10.1016/j.mssp.2015.12.018.

[14] Gödel, K. C., Y. C. Choi, B. Roose, A. Sadhanala, H. J. Snaith, S. I. Seok, U. Steiner, and S. K. Pathak, 2015, Efficient room temperature aqueous Sb2S3 synthesis for inorganic–organic sensitized solar cells with 5.1% efficiencies: Chemical Communications, **51**(41):8640–8643, doi:10.1039/C5CC01966D.

[15] Moon, S.-J., Y. Itzhaik, J.-H. Yum, S. M. Zakeeruddin, G. Hodes, and M. Grätzel, (2010) Sb2S3-Based Mesoscopic Solar Cell using an Organic Hole Conductor: The Journal of Physical Chemistry Letters, **1**(10):1524–1527, doi:10.1021/jz100308q.

[16] Choi, Y. C., D. U. Lee, J. H. Noh, E. K. Kim, and S. I. Seok, (2014) Highly Improved Sb2S3 Sensitized-Inorganic–Organic Heterojunction Solar Cells and Quantification of Traps by Deep-Level Transient Spectroscopy: Advanced Functional Materials, **24**(23):3587–3592, doi:10.1002/adfm.201304238.

[17] Du, H.-J., W.-C. Wang, and J.-Z. Zhu, (2016) Device simulation of lead-free CH 3 NH 3 SnI 3 perovskite solar cells with high efficiency: Chinese Physics B, **25**(10):108802, doi:10.1088/1674-1056/25/10/108802.

[18] Khoshsirat, N., and N. A. M. Yunus, (2013) Numerical simulation of CIGS thin film solar cells using SCAPS-1D, *in* 2013 IEEE Conference on Sustainable Utilization and Development in Engineering and Technology (CSUDET): 63–67, doi:10.1109/CSUDET.2013.6670987.

[19] Burgelman, M., P. Nollet, and S. Degrave, (2000) Modelling polycrystalline semiconductor solar cells: Thin Solid Films, **361–362**:527–532, doi:10.1016/S0040-6090(99)00825-1.

[20] Ben Nasr, T., H. Maghraoui-Meherzi, H. Ben Abdallah, and R. Bennaceur, (2011) Electronic structure and optical properties of Sb2S3 crystal: Physica B: Condensed Matter, **406**(2):287–292, doi:10.1016/j.physb.2010.10.070.

[21] Tumelero, M. A., R. Faccio, and A. A. Pasa, (2016) Unraveling the Native Conduction of Trichalcogenides and Its Ideal Band Alignment for New Photovoltaic Interfaces: The Journal of Physical Chemistry C, **120**(3):1390–1399, doi:10.1021/acs.jpcc.5b10233.

[22] Lee, D. U., S. Woo Pak, S. Gook Cho, E. Kyu Kim, and S. Il Seok, (2013) Defect states in hybrid solar cells consisting of Sb2S3 quantum dots and TiO2 nanoparticles: Applied Physics Letters, **103**(2):023901, doi:10.1063/1.4813272.

[23] Mostefaoui, M., H. Mazari, S. Khelifi, A. Bouraiou, and R. Dabou, (2015) Simulation of High Efficiency CIGS Solar Cells with SCAPS-1D Software: Energy Procedia, **74**:736–744, doi:10.1016/j.egypro.2015.07.809.

[24] Roy, B., B. R. Chakraborty, R. Bhattacharya, and A. K. Dutta, (1978) Electrical and magnetic properties of antimony sulphide (Sb2S3) crystals and the mechanism of carrier transport in it: Solid State Communications, 25(11):937–940, doi:10.1016/0038-1098(78)90306-X.